applied optics

3D nondestructive testing system with an affordable multiple reference optical-delay-based optical coherence tomography

Roshan Dsouza,[1] Hrebesh M. Subhash,[1,*] Kai Neuhaus,[1] Josh Hogan,[3] Carol Wilson,[3] and Martin Leahy[1,2]

[1]Tissue Optics and Microcirculation Imaging Group, School of Physics, National University of Ireland, Galway, Ireland
[2]Royal College of Surgeons (RCSI), Dublin, Ireland
[3]Compact Imaging, Inc., 897 Independence Ave., Suite 5B, Mountain View, California 94043, USA
*Corresponding author: hrebeshms@gmail.com

Received 17 March 2015; revised 18 May 2015; accepted 26 May 2015; posted 26 May 2015 (Doc. ID 236294); published 12 June 2015

Optical coherence tomography (OCT) is emerging as a powerful noncontact imaging technique, allowing high-quality cross-sectional imaging of scattering specimens nondestructively. However, the complexity and cost of current embodiments of an OCT system limit *its* use in various nondestructive testing (NDT) applications at resource-limited settings. In this paper, we demonstrate the feasibility of a novel low-cost OCT system for a range of nondestructive testing (NDT) applications. The proposed imaging system is based on an enhanced time-domain OCT system with a low cost and small form factor reference arm optical delay, called multiple reference OCT (MR-OCT), which uses a miniature voice coil actuator and a partial mirror for extending the axial scan range. The proposed approach is potentially a low-cost, compact, and unique optical imaging modality for a range of NDT applications in a low-resource setting. Using this method, we demonstrated the capability of MR-OCT to perform cross-sectional and volumetric imaging at 1200 A-scans per second.

OCIS codes: (110.0110) Imaging systems; (110.6880) Three-dimensional image acquisition; (120.4640) Optical instruments; (110.4500) Optical coherence tomography; (120.6650) Surface measurements, figure; (100.3175) Interferometric imaging.

http://dx.doi.org/10.1364/AO.54.005634

1. INTRODUCTION

Nondestructive testing (NDT) is a rapidly developing and redundant field comprising many different techniques and approaches. Over the past few decades, there have been tremendous advances in the field of NDT, including a wide range of new advanced sensors and sensing methodologies, which determine the physical properties, discontinuities, and differences in material characteristics in the scientific and industrial realms [1]. However, an NDT technology that enables noncontact, noninvasive, and high-resolution depth-resolved imaging in highly scattering material remains an unmet requirement. Optical coherence tomography (OCT) [2] is an emerging medical imaging technology based on low-coherence interferometry, which has been used to obtain cross-sectional images of tissue. Recently, the application of OCT has been extended to the diverse field of NDT, such as surface and subsurface characterization, measurement of layer thickness in multilayered foils [3], polymer science [4], printed circuit boards [5], solar cells [6], LEDs [7], and food products [8].

In general, an OCT system can be constructed either based on time-domain OCT (TD-OCT) or Fourier-domain OCT (FD-OCT). In TD-OCT, a depth scan is performed by moving a reference mirror, and FD-OCT is realized using a high-speed spectrometer [9] or a swept source (SS) laser source [10]. Typical implementation of an OCT system is based on a Michelson interferometer, which analyzes signals generated by the interference of backscattered light from a sample and reference reflection. OCT has become a well-established tool for many biomedical imaging applications, including ophthalmology [11], cardiology [12], dermatology [13], and dentistry [14]. However, the current embodiments of conventional OCT systems, either TD or FD, utilize large form-factor optical designs and are expensive, which restricts the use of OCT for a wide range of affordable NDT applications at a resource-limited setting.

In this paper, we introduce an affordable NDT imaging platform based on multiple reference OCT (MR-OCT), which is implemented with a novel concept described elsewhere

[15,16]. To achieve fast 3D imaging capability, we have improved the axial scanning frequency of the MR-OCT system to 600 Hz and utilize forward and backward sweeps to fully exploit the available scan rate. The working principle of the MR-OCT is similar to conventional TD-OCT, except an additional partial mirror is included in the MR-OCT. The partial mirror is placed close to the reference mirror (~95 μm), which is attached to an oscillating miniature actuator. The combination of the partial mirror and the oscillating reference mirror generates a composite reference signal based on multiple reflections between the partial mirror and the oscillating reference mirror. Our MR-OCT is based on (1) the movement of a single miniature actuator (such as a piezoelectric transducer, a voice coil actuator, or a vertical scanning MEMS), and (2) a partial mirror to generate multiple delayed scan segments. The magnitude of the scan segments increases with each order of reflection, as does the frequency of the associated interference signals, to provide extended axial scan range. The proposed optomechanical architecture of MR-OCT technology promises to fit into a robust and cost-effective design and may have the potential to be integrated as a solid-state design. Our research system works with a voice coil extracted from a CD/DVD-ROM pickup head (PUH). A complete PUH can be purchased for around $10 US [17]. The moderate scan speed also requires less-demanding computational hardware, and a compact, low-cost MR-OCT can be envisioned. Nevertheless, we can demonstrate 3D volume scans, even with low scan rates. This makes the MR-OCT a desirable system, which can be a novel, high-resolution addition to the diagnostic tools employed in NDT applications.

2. MATERIAL AND METHODS

A. MR-OCT System Setup

Figure 1 illustrates the experimental implementation of the MR-OCT based on a free-space Michelson interferometer with a voice-coil-based delay.

The light source is a broadband superluminescent diode at 1310 nm (l0) with 56 nm full width half-maximum bandwidth (Δl) (~15 mW optical power). In the reference arm, depth scanning is achieved by a miniature voice coil (VCM) actuator

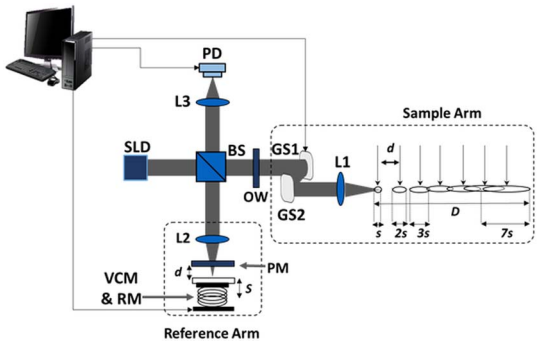

Fig. 1. Illustration of 3D MR-OCT system and imaging capabilities. Experimental configuration of the MR-OCT system based on bulk optics configuration. SLD, superluminescent diode; L1-L4, lenses; BS, beam splitter; PM, partial mirror; RM, reference mirror; VCM, voice coil motor; PD, photodetector; GS1-2, galvo scanner; OW, optical window; d, distance between PM and RM; s, scan range; D, total depth scan range.

extracted from a CD PUH. The drive frequency of the voice coil was 600 Hz, resulting in a scan rate 1200 scans per second and a scan range "s" of 60 μm. A partial mirror (PM) with 20% transmission efficiency is placed close to the reference mirror with a separation distance of ~95 μm. The sample arm consists of a pair of mirrors mounted onto galvanometer scanners, an optical window (OW) to compensate for the dispersion caused by the PM, and an objective lens with focal length of 50 mm to deliver the probe beam onto the sample. The measured axial imaging resolution and the transverse resolution of the system is ~13 and ~27 μm, respectively, in air. The reflected light from both arms is then detected by an InGaAs photodetector at the output of the interferometer. Next, the detected signal from the photodetector is low-pass filtered and then bandpass filtered based on the beat frequency of the first and nth order. The filtered analog MR-OCT signal is then digitized using a 12 bit A/D card and recorded on a workstation for further processing. The sensitivity of the system was measured by placing an optical density-3 filter in the sample arm as an attenuator and mirror as a test object. The measured sensitivity for the first order is 90 dB. There is a theoretical sensitivity drop of 0.97 dB for each successive MR-OCT order caused by 80/20 partial mirror reflectivity, and we experimentally observed a degradation of 1.1 dB per order.

B. MR-OCT Signal Processing

In order to reconstruct the MR-OCT image, a custom algorithm was developed in MATLAB. The developed algorithm utilizes forward and backward sweeps of the axial scans to reconstruct the MR-OCT image. As a first step of reconstruction, the nonlinearity of the raw interferograms caused by the sinusoidal axial scanning is corrected based on a lookup table, which relates to the actual movement of the scan mirror. Next, the linearized raw interferograms were filtered using a polyphase IIR bandpass filter bank based on Chebyshev type 2 IIR design. The separated orders were then stored in different signal channels. After filtering each order, the envelopes of the interferograms were detected using an algorithm based on the Hilbert transform. Finally, the rescaled scan segments corresponding to each of the MR-OCT orders are stitched together according to their actual depth positions within the image matrix to form a depth-resolved MR-OCT A-line. In this experiment, the first 12 orders were used to reconstruct the MR-OCT A-line with a total scan range, D, of 1.4 mm in air.

3. RESULTS AND DISCUSSION

A. Evaluating the Geometry of Micromechanical Components

Surface texture plays a vital role in the functionality of a component. Typical surface analysis yields the roughness and structural information of micromechanical components, which are produced industrially. This information is pivotal in assessing the component performance. The importance of these analyses resides, therefore, in the fact that they guarantee the quality of the produced components while also maximizing production efficiency. Optical profilometry-based methods have been used to analyze the structural defects of the components due to their noncontact, high-accuracy features [18,19]. Light microscopy

typically will suffer from reflections for reflective surfaces and overcasting geometrical features. Profilometers can achieve large depth scans depending on the structural geometry of the surface but cannot be used to profile subsurface features of semitransparent materials. MR-OCT has shown itself to be the better tool in our geometrical analysis. It should be most useful for low-volume, high-precision, and on-demand development of complex geometrical structures. We imaged a metal screw over an area of 3 mm × 3 mm to analyze the structural information. A 3D volume recording was taken, which contained a total frame with 300 A-lines per B-frame. Figure 2(a) shows the 3D rendering of the metal screw. Figure 2(b) shows the *en face* view of the metal screw from XZ slices at varying depths. Figure 2[b(i)] shows the slice at a depth of 60 μm; Fig. 2[b(ii)] at 170 μm; Fig. 1[b(iii)] at 300 μm; and Fig. 2[b(iv)] at 400 μm. A supporting flythrough movie of the volume data is also provided (see Media 1).

B. Nondestructive 3D Imaging of Coated Capsule

The coating of pharmaceutical tablets is reported to be of major interest to the pharmaceutical industry [20]. The thickness, consistency, and uniformity of the tablet coating must be precisely controlled to ensure the encapsulated drugs are released within a specified therapeutic window. Scanning electron microscopy [21] and atomic force microscopy [22] have been demonstrated to measure the surface morphology and surface uniformity; however, these systems are bulky, very slow, and highly expensive. OCT has been used to investigate the thickness and homogeneity of pharmaceutical tablets [23,24]. Here, we demonstrate the MR-OCT capabilities for imaging these tablets. For investigation purposes, we imaged the coated capsule of a multivitamin capsule over an area of 3 mm × 3 mm with MR-OCT. A total recording of 300 B-frames with 300 A-lines per B-frame was performed to reconstruct a 3D volume. Figure 3(a) shows the 3D rendering of the coated capsule (Media 2). Figure 3(b) shows the *en face* view of the tablet from XZ slices at varying depths. Figure 3[b(i)] shows the slice at a depth of 190 μm; Fig. 3[b(ii)] at 330 μm; and Fig. 3[b(iii)] at 455 μm. A supporting flythrough movie of the volume data is also provided (see Media 2). MR-OCT has the potential to perform monitoring during the production process due to low-cost, highly accurate measurement.

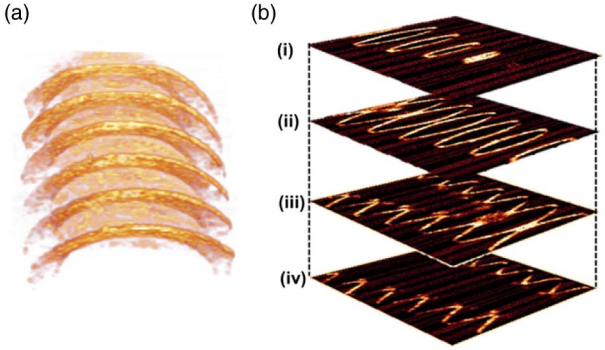

Fig. 2. 3D optical profiling of a metal screw (Media 1). (a) 3D volume rendering of a metal screw. (b) Series of *en face* views (XZ) at varying depths through the sample: (i) 60 μm; (ii) 170 μm; (iii) 300 μm; (iv) 400 μm.

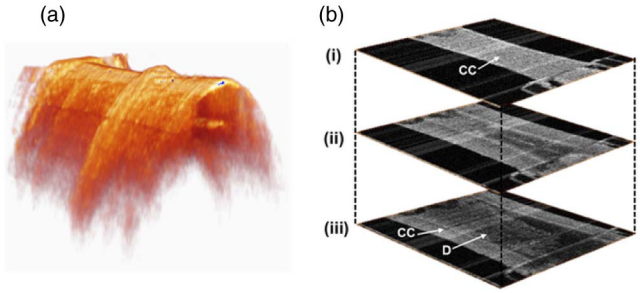

Fig. 3. 3D reconstruction of the coated capsule (Media 2). (a) 3D volume rendering of a coated capsule. (b) Series of *en face* views (XZ) at varying depths through the sample (i) 190 μm; (ii) 330 μm; (iii) 455 μm. CC, capsule coating; D, drug.

C. Nondestructive 3D Imaging of Textile Materials

In a competitive textile market, quality management plays a crucial role. Fabric defects can be caused during any process on the production line. Manual inspection of textiles to detect defects is not only time consuming, it is subject to human error and does not promote a streamlined production process. Several methods have been reported for defect detection in different fabric [25]. There have also been some OCT-based studies, which have shown detailed quantification of textile materials and examined their influence on human skin [26,27]. In our study, we used the MR-OCT system to investigate a fabric material based on polyester. The imaging area on the fabric was 3 mm × 3 mm. The MR-OCT 3D data volume contained a total of 300 B-frames with 300 A-lines per B-frame. The total imaging time for the 3D acquisition was approximately 153 s. Figure 4(a) shows the 3D rendering of the MR-OCT fabric with various structural features. To allow for a better assessment of the depth structure of fabric, an *en face* view from XZ slices are shown in Fig. 4(b) at varying depths through the sample. Figure 4[b(i)] shows the slice at a depth of 77 μm; Fig. 4[b(ii)] at 245 μm; and Fig. 4[b(iii)] at 350 μm. A supporting flythrough movie of the volume data is also provided (see Media 3).

D. Nondestructive 3D Inspection of Liquid Crystal Panels

Liquid crystal (LC) panels have been widely used as spatial light modulators for display and imaging applications. During the manufacturing process, quality check for LC panels plays a vital role for measuring parameters such as thickness, roughness,

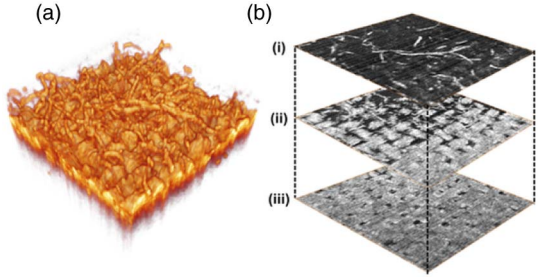

Fig. 4. 3D reconstruction of the textile material (Media 3). (a) 3D volume rendering of a textile material. (b) Series of *en face* views (XZ) at varying depths through the sample: (i) 77 μm; (ii) 245 μm; (iii) 350 μm.

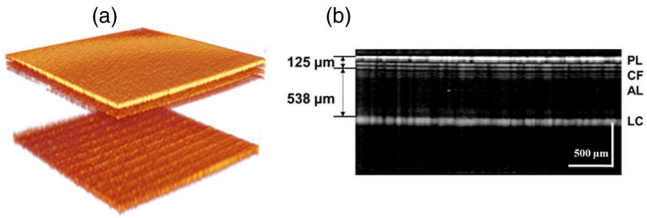

Fig. 5. 3D reconstruction of the LC panel. (a) 3D volume rendering of a LC panel. (b) Cross-sectional image of an LC panel. PL, polarizer; CF, color filter; AL, alignment layer; LC, liquid crystal.

or defects such as voids. Visual or CCD-based techniques have been used for defect inspection; however, such techniques can detect defects only in horizontal locations [28,29]. OCT is an effective way to perform defect inspection in LC panels due to advantages such as high resolution and increased penetration depth for semitransparent materials. Studies have shown OCT being used to investigate the vertical location of defects within the LC panels [30,31]. We used the MR-OCT system to analyze the layers and structural information of an LC panel. The imaging area on the LC panel was 3 mm × 3 mm. The MR-OCT 3D data volume contained a total of 300 B-frames with 300 A-lines per B-frame. Figure 5(a) shows the 3D rendering of the LC panel, and Fig. 5(b) shows the B-frame of the LC panel clearly showing the depth layers.

4. CONCLUSION

We have demonstrated the feasibility of MR-OCT for affordable NDT applications for resource-limited settings. We have advanced the imaging speed and system capability of MR-OCT for 3D NDT imaging application. To achieve reasonable 3D imaging speed for NDT applications, we have improved the axial scanning frequency to 600 Hz and utilized forward and backward scans to obtain a scan rate of 1200 A scans/s. With moderate spatial resolution and good system sensitivity of the MR-OCT system presented here, we have completed an accurate structural analysis for NDT applications. Due to the compactness and simplicity of MR-OCT architecture, the interferometric part of MR-OCT system could be implemented based on the optical pickup unit of a DVD player at a small fraction of the cost of a normal OCT system. Moreover, due to the moderate scan speed, a low-cost mobile platform will be feasible for instrumentation and computational needs. Although the imaging speed of MR-OCT is limited in comparison to latest FD-OCT system, the system sensitivity and imaging parameters are well enough for addressing a wide range of affordable NDT applications at resource-limited settings and small-scale industries. Furthermore, there is room to increase the sensitivity of the MR-OCT system by eliminating the 80% reflection caused by the partial mirror using a polarization-based design.

Galway University Foundation; Irish Government and the European Union; National Biophotonics Imaging Platform (NBIP) Ireland; University of Limerick Foundation.

the National Biophotonics Imaging Platform (NBIP) Ireland is funded under the Higher Education Authority PRTLI Cycle 4, co-funded by the Irish Government and the European Union – Investing in your future, and Compact Imaging, Inc. All authors have a financial interest in Compact Imaging, Inc.

REFERENCES

1. Y. K. Zhu, G. Y. Tian, R.-S. Lu, and H. Zhang, "A review of optical NDT technologies," Sensors **11**, 7773–7798 (2011).
2. A. F. Fercher, W. Drexler, C. K. Hitzenberger, and T. Lasser, "Optical coherence tomography–principles and applications," Rep. Prog. Phys. **66**, 239–303 (2003).
3. K. Wiesauer, M. Pircher, E. Götzinger, S. Bauer, R. Engelke, G. Ahrens, G. Grützner, C. Hitzenberger, and D. Stifter, "En-face scanning optical coherence tomography with ultra-high resolution for material investigation," Opt. Express **13**, 1015–1024 (2005).
4. P. Meemon, J. Yao, K.-S. Lee, K. P. Thompson, M. Ponting, E. Baer, and J. P. Rolland, "Optical coherence tomography enabling non destructive metrology of layered polymeric GRIN material," Sci. Rep. **3**, 2045–2322 (2013).
5. J. Czajkowski, T. Prykäri, E. Alarousu, J. Palosaari, and R. Myllylä, "Optical coherence tomography as a method of quality inspection for printed electronics products," Opt. Rev. **17**, 257–262 (2010).
6. L. Thrane, T. M. Jørgensen, M. Jørgensen, and F. C. Krebs, "Application of optical coherence tomography (OCT) as a 3-dimensional imaging technique for roll-to-roll coated polymer solar cells," Sol. Energy Mater. Sol. Cells **97**, 181–185 (2012).
7. N. H. Cho, U. Jung, S. Kim, and J. Kim, "Non-destructive inspection methods for LEDs using real-time displaying optical coherence tomography," Sensors **12**, 10395–10406 (2012).
8. I. V. Meglinski, C. Buranachai, and L. A. Terry, "Plant photonics: application of optical coherence tomography to monitor defects and rots in onion," Laser Phys. Lett. **7**, 307–310 (2010).
9. R. Leitgeb, C. Hitzenberger, and A. Fercher, "Performance of Fourier domain vs. time domain optical coherence tomography," Opt. Express **11**, 889–894 (2003).
10. M. Choma, M. Sarunic, C. Yang, and J. Izatt, "Sensitivity advantage of swept source and Fourier domain optical coherence tomography," Opt. Express **11**, 2183–2189 (2003).
11. M. R. Hee, C. A. Puliafito, J. S. Duker, E. Reichel, J. G. Coker, J. R. Wilkins, J. S. Schuman, E. A. Swanson, and J. G. Fujimoto, "Topography of diabetic macular edema with optical coherence tomography," Ophthalmology **105**, 360–370 (1998).
12. H. Yabushita, B. E. Bouma, S. L. Houser, H. T. Aretz, I.-K. Jang, K. H. Schlendorf, C. R. Kauffman, M. Shishkov, D.-H. Kang, E. F. Halpern, and G. J. Tearney, "Characterization of human atherosclerosis by optical coherence tomography," Circulation **106**, 1640–1645 (2002).
13. M. C. Pierce, J. Strasswimmer, B. H. Park, B. Cense, and J. F. de Boer, "Advances in optical coherence tomography imaging for dermatology," J. Invest. Dermatol. **123**, 458–463 (2004).
14. L. L. Otis, M. J. Everett, U. S. Sathyam, and B. W. Colston, "Optical coherence tomography: a new imaging technology for dentistry," J. Am. Dent. Assoc. **131**, 511–514 (2000).
15. J. Hogan, "Multiple reference non-invasive analysis system," U. S. patent WO2006023634 A3 (9 April 2009).
16. R. Dsouza, H. Subhash, K. Neuhaus, J. Hogan, C. Wilson, and M. Leahy, "Dermascope guided multiple reference optical coherence tomography," Biomed. Opt. Express **5**, 2870–2882 (2014).
17. A. Kasukurti, M. Potcoava, S. A. Desai, C. Eggleton, and D. W. M. Marr, "Single-cell isolation using a DVD optical pickup," Opt. Express **19**, 10377–10386 (2011).
18. T. G. Mathia, P. Pawlus, and M. Wieczorowski, "Recent trends in surface metrology," Wear **271**, 494–508 (2011).
19. N. P. Avdelidis, E. T. Delegou, D. P. Almond, and A. Moropoulou, "Surface roughness evaluation of marble by 3D laser profilometry and pulsed thermography," NDT & E Int. **37**, 571–575 (2004).
20. A. Palou, J. Cruz, M. Blanco, J. Tomàs, J. de los Ríos, and M. Alcalà, "Determination of drug, excipients and coating distribution in pharmaceutical tablets using NIR-CI," J. Pharm. Biomed. Anal. **2**, 90–97 (2012).

21. P. Seitavuopio, J. Heinämäki, J. Rantanen, and J. Yliruusi, "Monitoring tablet surface roughness during the film coating process," AAPS Pharm. Sci. Tech. **7**, E1–E6 (2006).
22. T. Li and K. Park, "Fractal analysis of pharmaceutical particles by atomic force microscopy," Pharm. Res. **15**, 1222–1232 (1998).
23. J. M. A. Mauritz, R. S. Morrisby, R. S. Hutton, C. H. Legge, and C. F. Kaminski, "Imaging pharmaceutical tablets with optical coherence tomography," J. Pharm. Sci. **99**, 385–391 (2010).
24. D. M. Koller, G. Hannesschläger, M. Leitner, and J. G. Khinast, "Non-destructive analysis of tablet coatings with optical coherence tomography," Eur. J. Pharm. Sci. **44**, 142–148 (2011).
25. H. Y. T. Ngan, G. K. H. Pang, and N. H. C. Yung, "Automated fabric defect detection—a review," Image Vis. Comput. **29**, 442–458 (2011).
26. H. Strese, M. Kuck, R. Benken, S. Schanzer, H. Richter, J. W. Fluhr, M. C. Meinke, C. Benderoth, G. Frankowski, W. Sterry, and J. Lademann, "Application of optical methods to characterize textile materials and their influence on the human skin," J. Biomed. Opt. **16**, 046013 (2011).
27. H. Strese, M. Kuck, R. Benken, J. W. Fluhr, S. Schanzer, H. Richter, M. C. Meinke, J. Beuthan, C. Benderoth, G. Frankowski, W. Sterry, and J. Lademann, "Influence of finishing textile materials on the reduction of skin irritations," Skin. Res. Technol. **19**, e409–e416 (2013).
28. Y. Mori, K. Tanahashi, and S. Tsuji, "Quantitative evaluation of 'mura' in liquid crystal displays," Opt. Eng. **43**, 2696–2700 (2004).
29. J. Y. Lee and S. I. Yoo, "Automatic detection of region-mura defect in TFT-LCD," IEICE Trans. Info. Sys. **E87-D**, 2371–2378 (2004).
30. S. H. Kim, J. H. Kim, and S. W. Kang, "Nondestructive defect inspection for LCDs using optical coherence tomography," Displays **32**, 325–329 (2011).
31. C. C. Tsai, Y. S. Lin, S. C. Pei, C. K. Chang, T. H. Chen, N. C. Cheng, M. K. Tsai, C. C. Lai, W. Y. Li, C. K. Wei, and S. L. Huang, "Microstructural and microspectral characterization of a vertically aligned liquid crystal display panel," Opt. Lett. **36**, 567–569 (2011).